Supplement of Atmos. Chem. Phys., 23, 5335–5353, 2023
https://doi.org/10.5194/acp-23-5335-2023-supplement

Atmospheric Chemistry and Physics
Open Access

Supplement of

On the magnitude and sensitivity of the quasi-biennial oscillation response to a tropical volcanic eruption

Flossie Brown et al.

Correspondence to: Flossie Brown (fb428@exeter.ac.uk)

Supplementary Information

Supplementary Text S1: Modified dynamics in the 2D dynamical model

The equations (2)-(1) in the main text can be regarded as a way of calculating $\frac{\partial u}{\partial t}$ and $\frac{\partial T}{\partial t}$ given all other variables. (This is required in any calculation of the evolution of u and T.) Note that (3) and (4) can be differentiated with respect to t and combined to give a linear relation between $\frac{\partial u}{\partial t}$ and $\frac{\partial T}{\partial t}$ and (5) can be used to write each of v and w in terms of a streamfunction ψ. Then we have three coupled equations, represented symbolically as:

$$\frac{\partial u}{\partial t} + A_u\,\psi = G[u] \qquad (8)$$

$$\frac{\partial T}{\partial t} + A_T\,\psi = Q_{volc} + Q_{rad}[T] \qquad (9)$$

$$\varepsilon_u \frac{\partial u}{\partial t} + \varepsilon_T \frac{\partial T}{\partial t} = 0 \qquad (10)$$

These equations are not linear because the operators and some of the quantities on the right depend on u and on T. But at any instant $\frac{\partial u}{\partial t}$, $\frac{\partial T}{\partial t}$ and ψ are linear functions of the terms on the right-hand side, including Q_{volc} and G. Consider $A_u\,\psi$, which represents the terms including v and w in (2). Divide these into two parts ${A_u}^{(l)}\psi$ representing the Coriolis force $-2\Omega\,sin\varphi\,v$ and ${A_u}^{(nl)}\psi$ representing the advection of relative momentum by the residual mean circulation. ${A_u}^{(nl)}\psi$ is the term that is responsible for the asymmetry between easterly and westerly shear zones in the QBO. ${A_u}^{(l)}\psi$ is the term that is included in all linear descriptions of the residual circulation and which allows, for example, the response to an applied heating to be distributed between a response in temperature and a response in velocity.

Now separate the above equations into two parts:

$$\frac{\partial u^{(1)}}{\partial t} + {A_u}^{(1)}\,\psi^{(1)} = G[u] \qquad (11)$$

$$\frac{\partial T^{(1)}}{\partial t} + A_T\,\psi^{(1)} = Q_{rad}[T^{(1)}] \qquad (12)$$

$$\varepsilon_u \frac{\partial u^{(1)}}{\partial t} - \varepsilon_T \frac{\partial T^{(1)}}{\partial t} = 0 \qquad (13)$$

$$\frac{\partial u}{\partial t} + {A_u}^{(2)}\,\psi^{(2)} = 0 \qquad (14)$$

$$\frac{\partial T^{(2)}}{\partial t} + A_T\,\psi^{(2)} = Q_{volc} + Q_{rad}[T^{(2)}] \qquad (15)$$

$$\varepsilon_u \frac{\partial u^{(2)}}{\partial t} - \varepsilon_T \frac{\partial T^{(2)}}{\partial t} = 0 \qquad (16)$$

The $u^{(1)}$, $u^{(2)}$, $T^{(1)}$ and $T^{(2)}$ fields are followed in time, with the relation $u = u^{(1)} + u^{(2)}$and $T = T^{(1)} + T^{(2)}$ being applied at all times (in particular to define the *A* operators).

If ${A_u}^{(1)} = {A_u}^{(2)} = A_u$, then the separation will have no effect. The evolution of u and T will be exactly as it was according to the original unseparated equation. (It has been verified that the numerical implementation satisfies this property.)

If ${A_u}^{(1)} = {A_u}^{(2)} = {A_u}^{(l)}$, then the effect of the separation will be the same as solving the original equations with $A_u = {A_u}^{(l)}$, i.e., the dynamics will be linear in the sense that no advection of relative momentum is taken into account. (The result will be that there is no asymmetry of QBO shear zones.)

If ${A_u}^{(1)} = A_u$ and ${A_u}^{(2)} = {A_u}^{(l)}$, then advection of relative momentum by the part of the meridional circulation induced directly by the aerosol heating will be neglected, but advection of relative momentum by the remaining part of the meridional circulation will be included. This defines the modified dynamics. The results of applying the modified dynamics to the QBO perturbation simulations are shown Figure 8. See main text for discussion.

Supplementary Text S2: Results from eruptions in January

Figure S1 shows the QBO zonal mean winds for eruptions in January (cf. Fig. 3 in the main text). We identify the same trends as outlined for July eruptions; the e-QBO is more disrupted than the w-QBO in response to a tropical eruption. Considering the response to eruptions in January in greater detail, we find a 60 Tg eruption causes the QBO phases to ascend after an eruption initiated in both a w-QBO and an e-QBO state, but 15 Tg eruptions do not cause observable ascent. Even so, the westerly phase is substantially delayed in the lower stratosphere after a 15 Tg eruption initiated during an e-QBO such that the easterly phase above descends 12 months later than in the control simulation (comparable to the delay of the 15 Tg case in July). Minor differences between the responses to an eruption in January compared to July are expected since the initial conditions including the QBO are not identical, but we conclude that the season of eruption does not noticeably affect the progression of the QBO.

Figure S2 shows the latitudinal position of the QBO westerly phase after eruptions in January (cf. Fig. 5, Sect. 3.1.3). The westerly phase of the QBO after a 60 Tg eruption initiated during a w-QBO state deviates substantially from the control simulations until 15 months after the eruption. The most notable change relative to the control is an excursion to 12° S after 5 months. A strengthening of the westerly phase in the Southern Hemisphere can also be identified in Fig. S6e. Importantly, the movement of the QBO away from the equator occurs in the opposite hemisphere to an eruption in July, but is otherwise similar in magnitude. After a 15 Tg eruption initiated during a w-QBO state in January, there are no significant changes.

Both 15 Tg and 60 Tg eruptions initiated during an e-QBO state show movement into the Southern Hemisphere compared to the control simulations, reaching 6° S and 9° S, respectively. This latitudinal movement following the e-QBO state is larger than shown for the July eruptions, possibly because the initial QBO state is slightly different due to the natural variability of the QBO. For example, the westerly phase is stronger and extends to higher altitudes at the start of the simulation for the case chosen in January (cf. Fig. 9e and Fig. S5e). i.e. the w-QBO and e-QBO states selected for the January simulations are more similar to each other than the corresponding w-QBO and e-QBO states chosen for the July simulations. This may make the January case more sensitive to movement as the westerly phase is initially located above the temperature anomaly, or it may affect the aerosol distribution and subsequent feedbacks.

To further understand the changes in the QBO latitudinal structure, a comparison of latitudinal variation in sAOD 5 months after an eruption is shown in Fig. S4. We confirm that for an eruption during a w-QBO in January there is a steep decline in sAOD in the Southern Hemisphere, opposite to the sAOD pattern seen for an equivalent eruption in July. We also confirm that the sAOD for eruptions initiated during an e-QBO are more symmetrical than for the w-QBO. Finally, we show that

for eruptions initiated in January, the e-QBO and w-QBO sAOD pattern are more similar than for the corresponding eruptions initiated in July. This may explain why the latitudinal movement predicted for eruptions in January are similar in magnitude and direction whereas for eruptions in July there is only a strong response seen during w-QBO initial conditions (Fig. 5). Further ensemble members with a variety of e-QBO states would be needed to confirm if the differences between the e-QBO latitudinal response in January and July is due to the season or natural variability among e-QBO states.

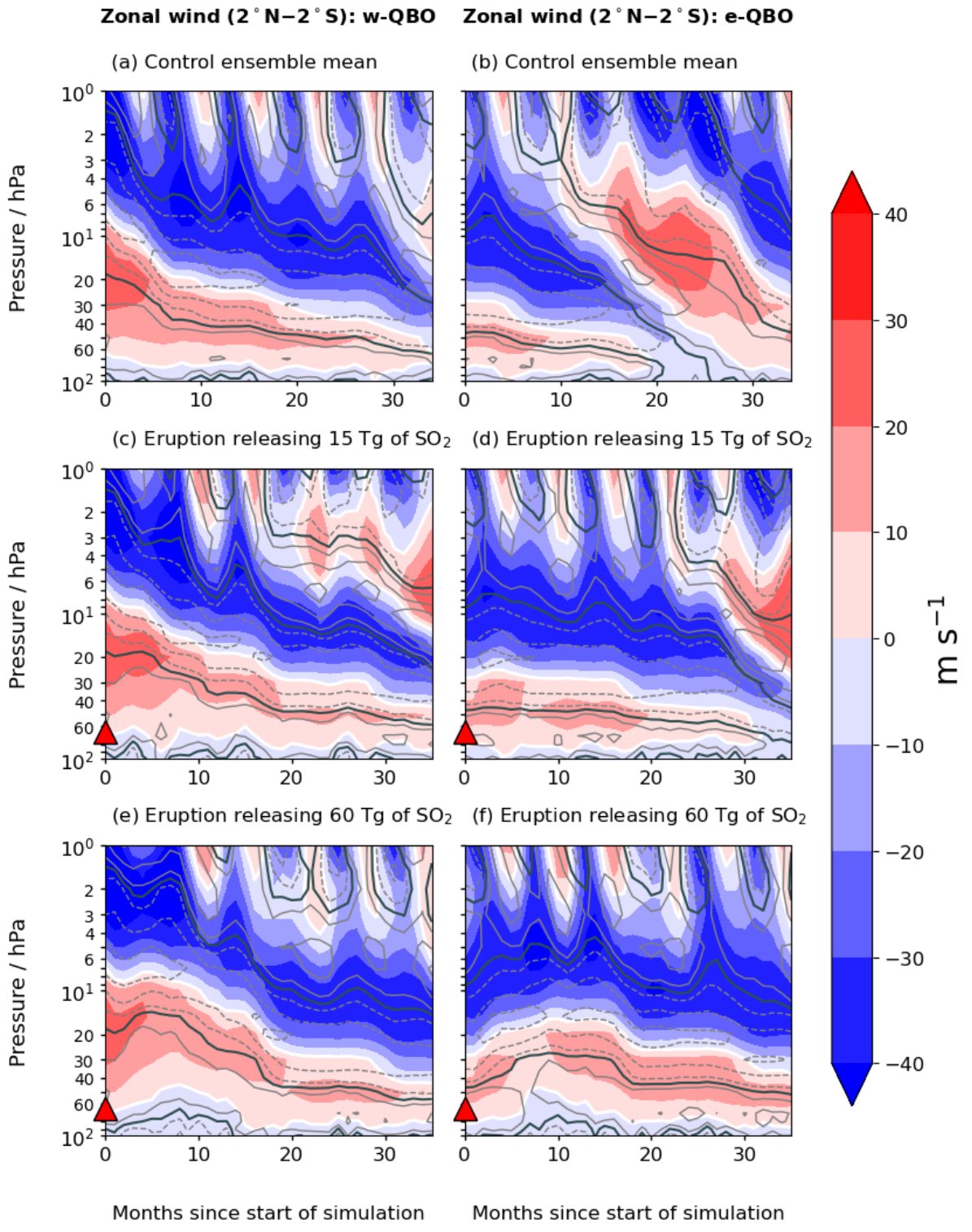

Figure S1: Filled contours: Mean zonal wind averaged 2° N – 2° S. Contour lines: Positive (solid) and negative (dashed) mean zonal wind shear (the change in wind speed with height) at intervals of 0.0025 s^{-1} averaged 2° N – 2° S. A black solid contour indicates a wind shear of zero. The left column shows simulations initiated during westerly QBO shear at 30 hPa, and the right column shows simulations initiated during easterly shear at 30 hPa for (a, b) the control ensemble mean (3 members), (c, d) 15 Tg eruptions, (e, f) 60 Tg eruptions. A white solid contour indicates the zero-wind line. Red triangles indicate the approximate altitude of SO_2 injection.

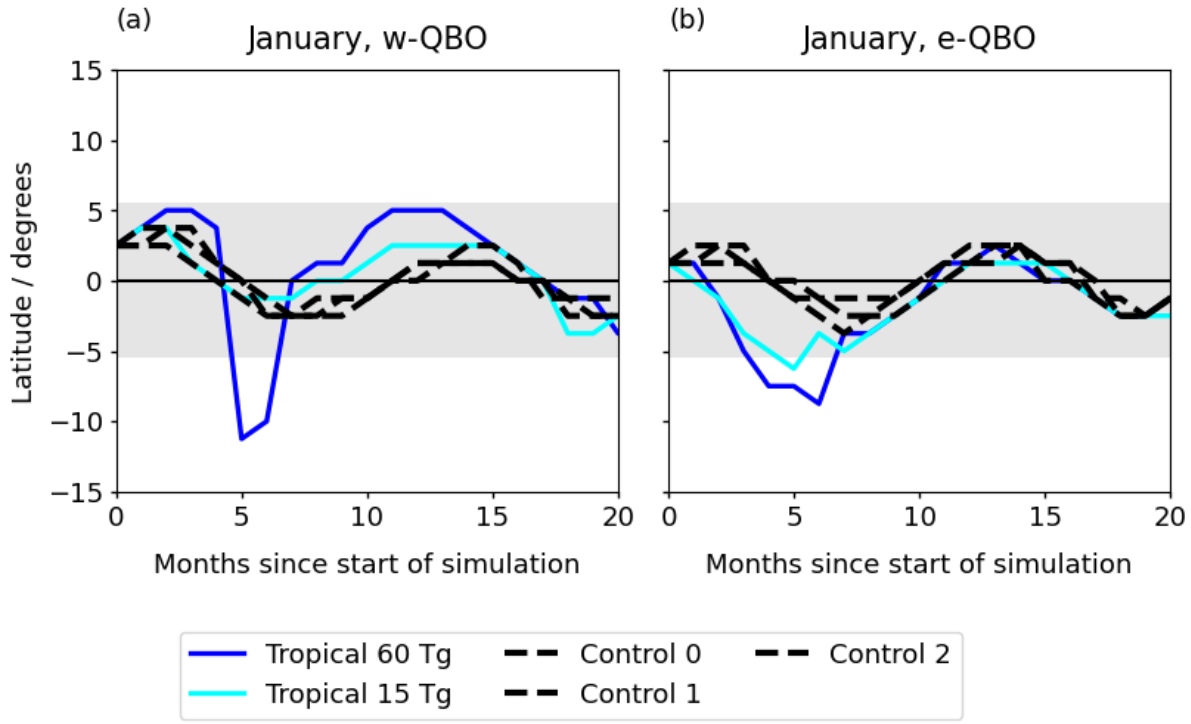

Figure S2: Latitudinal structure of the QBO for (a) eruptions initiated during a w-QBO and (b) eruptions initiated during an e-QBO. Solid lines indicate latitudinal position of the QBO westerly wind maximum in the region 10 hPa – 70 hPa, 15° N – 15° S following 60 Tg and 15 Tg eruptions and black dashed lines indicate the latitudinal position of the QBO westerly wind maximum for each of the three control ensemble members. Grey shading covers the latitudes that contain 95% of the variation in the position of the observed QBO westerly maximum.

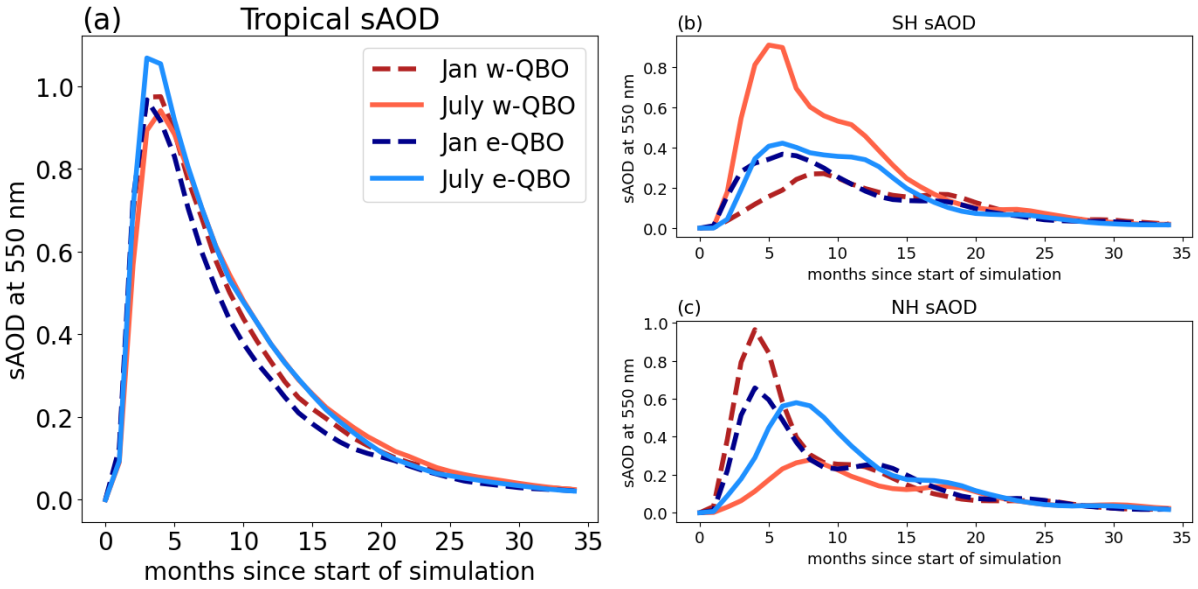

Figure S3: SAOD at 550 nm over time for (a) the tropics (30° N – 30° S), (b) the Southern Hemisphere (30° S – 90° S) and (c) the Northern hemisphere (30° N – 90° N).

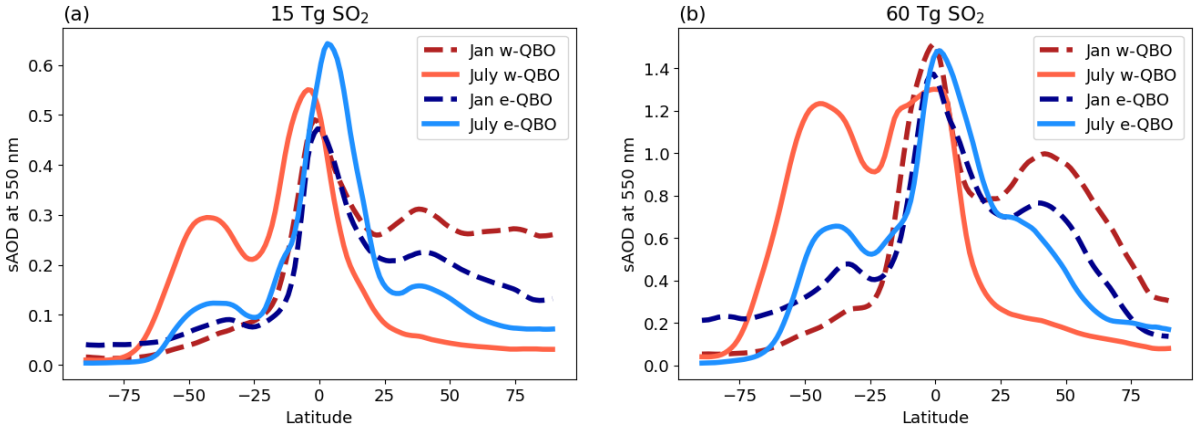

Figure S4: A latitudinal cross-section of sAOD at 550 nm 5 months after an eruption for each set of initial conditions for (a) 15 Tg eruptions and (b) 60 Tg eruptions.

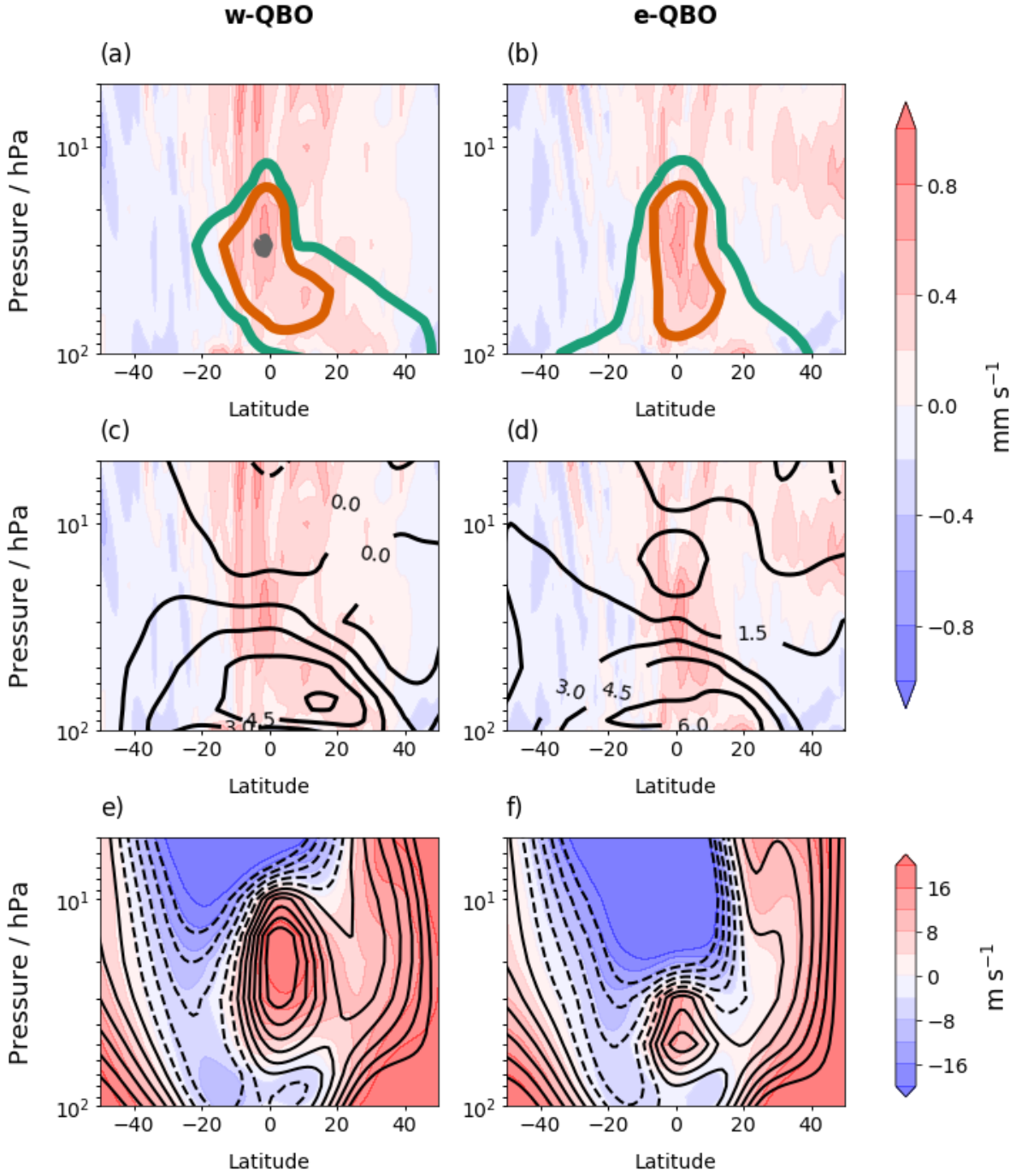

Figure S5: Two months after 60 Tg eruptions in January: (a), (b) shows the *w* anomalies (filled contours) and sulfate mass mixing ratio anomalies (coloured line contours) with respect to the control ensemble mean and (c), (d) shows the *w* anomalies (filled contours) and positive temperature anomalies (black solid contours). The sulfate mass mixing ratio contours are at interval of 5 x10^{-8}, 15 x10^{-8}, 50 x10^{-8} kg kg^{-1} and the temperature contours are in intervals of 1.5 K. Panels (e), (f) show the monthly mean zonal wind after the eruption (filled contours) compared to the control (black contours). The filled contour intervals are the same as the line contours, with dashed lines representing negative zonal winds in the line contours. Panels (a), (c) and (e) show results for the w-QBO, and panels (b), (d) and (f), for the e-QBO.

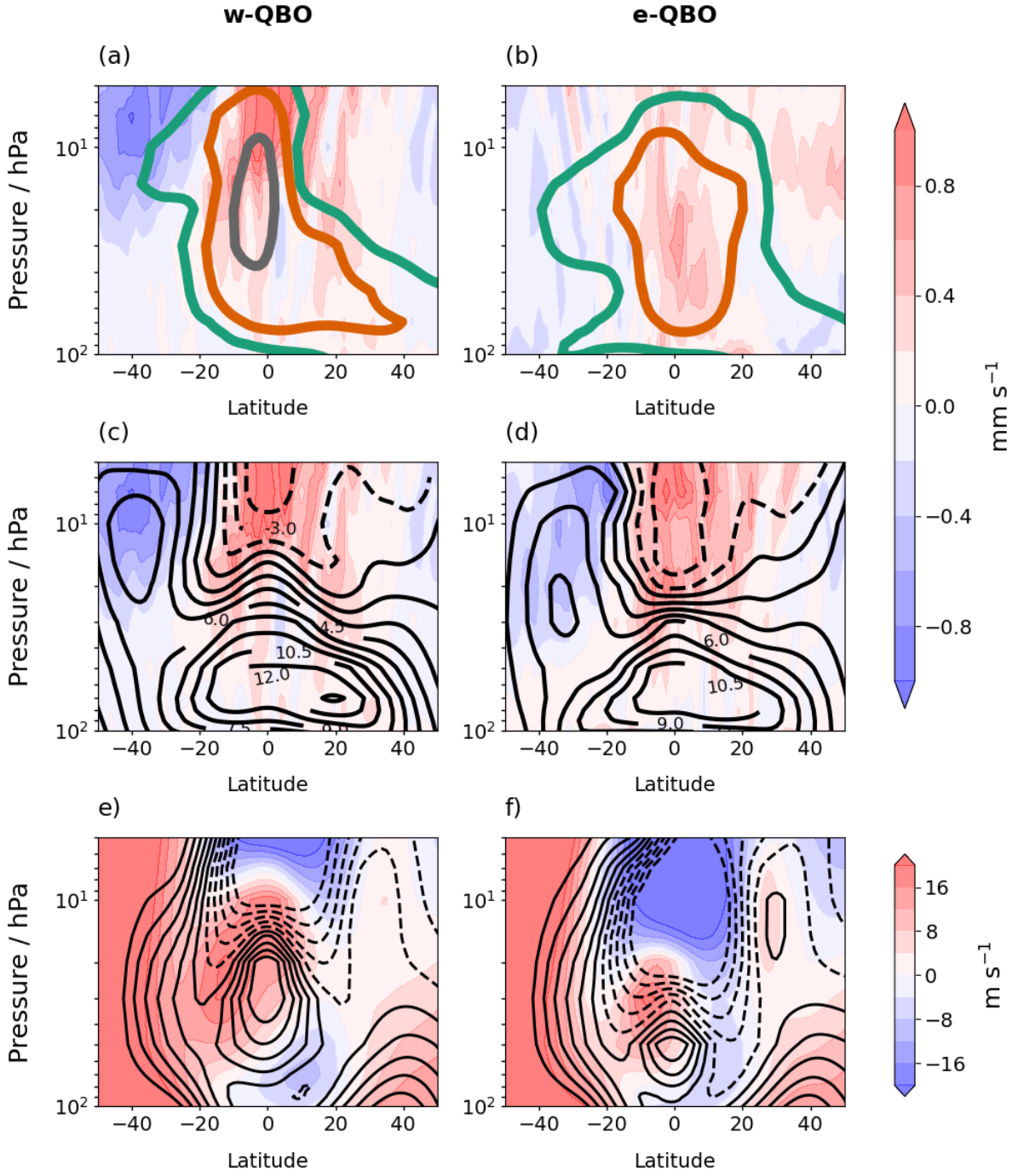

Figure S6: Five months after 60 Tg eruptions in January: (a), (b) shows the *w* anomalies (filled contours) and sulfate mass mixing ratio anomalies (coloured line contours) with respect to the control ensemble mean and (c), (d) shows the *w* anomalies (filled contours) and positive temperature anomalies (black solid contours). The sulfate mass mixing ratio contours are at interval of 5 x10^{-8}, 15 x10^{-8}, 50 x10^{-8} kg kg^{-1} and the temperature contours are in intervals of 1.5 K. Panels (e), (f) show the monthly mean zonal wind after the eruption (filled contours) compared to the control (black contours). The filled contour intervals are the same as the line contours, with dashed lines representing negative zonal winds in the line contours. Panels (a), (c) and (e) show results for the w-QBO, and panels (b), (d) and (f), for the e-QBO.

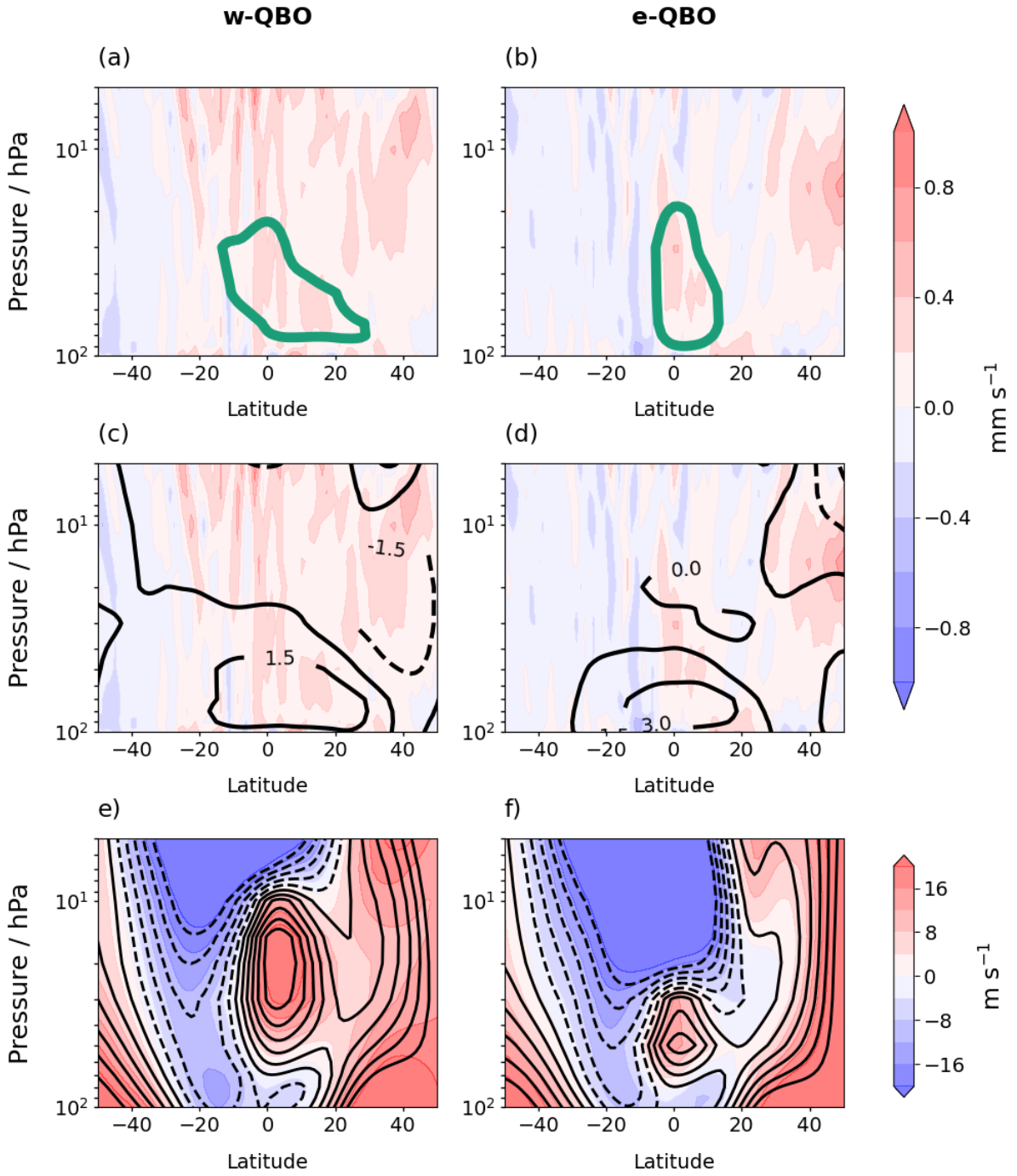

Figure S7: Two months after 15 Tg eruptions in January: (a), (b) shows the *w* anomalies (filled contours) and sulfate mass mixing ratio anomalies (coloured line contours) with respect to the control ensemble mean and (c), (d) shows the *w* anomalies (filled contours) and positive temperature anomalies (black solid contours). The sulfate mass mixing ratio contours are at interval of 5 x10^{-8}, 15 x10^{-8}, 50 x10^{-8} kg kg^{-1} and the temperature contours are in intervals of 1.5 K. Panels (e), (f) show the monthly mean zonal wind after the eruption (filled contours) compared to the control (black contours). The filled contour intervals are the same as the line contours, with dashed lines representing negative zonal winds in the line contours. Panels (a), (c) and (e) show results for the w-QBO, and panels (b), (d) and (f), for the e-QBO.

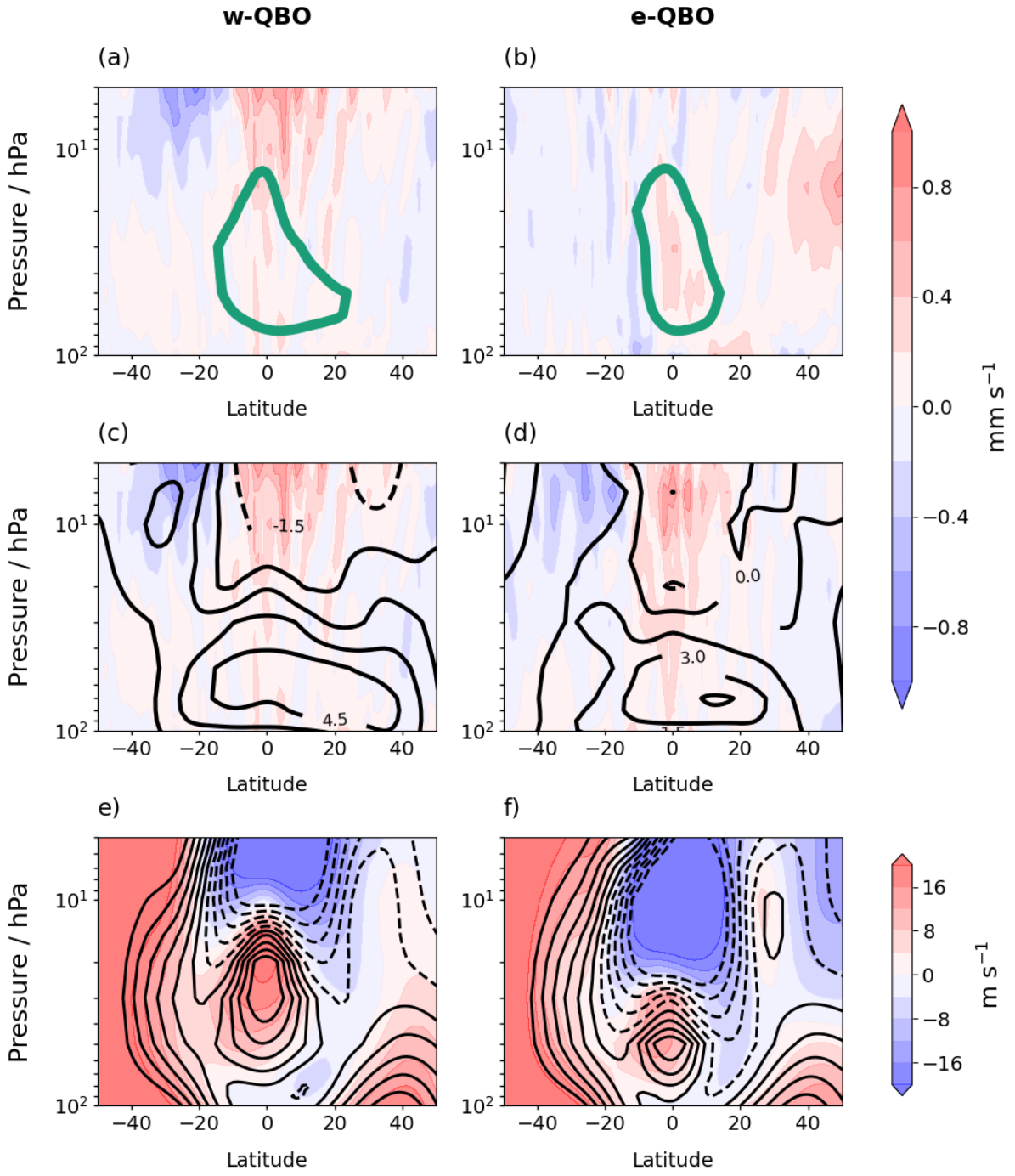

Figure S8: Five months after 15 Tg eruptions in January: (a), (b) shows the *w* anomalies (filled contours) and sulfate mass mixing ratio anomalies (coloured line contours) with respect to the control ensemble mean and (c), (d) shows the *w* anomalies (filled contours) and positive temperature anomalies (black solid contours). The sulfate mass mixing ratio contours are at interval of 5 x10^{-8}, 15 x10^{-8}, 50 x10^{-8} kg kg^{-1} and the temperature contours are in intervals of 1.5 K. Panels (e), (f) show the monthly mean zonal wind after the eruption (filled contours) compared to the control (black contours). The filled contour intervals are the same as the line contours, with dashed lines representing negative zonal winds in the line contours. Panels (a), (c) and (e) show results for the w-QBO, and panels (b), (d) and (f), for the e-QBO.

Supplementary Text 3: Results for 15 Tg eruptions in July

As for the 60 Tg eruptions (Fig. 9 of the main text), initial transport of sulfate after a 15 Tg injection is strongest into the Southern Hemisphere following an eruption initiated during a w-QBO state, but for the e-QBO state the sulfate distribution is more symmetrical (Fig. S9). After five months the aerosol has begun to decay and the month with the highest burden has already passed, due to the smaller SO_2 injection and thus smaller volcanic aerosol burden compared to a 60 Tg eruption (Fig. S10). The bulk of the volcanic sulfate aerosol is still located in the Southern Hemisphere although there is increased transport into the Northern Hemisphere (Fig. S10a, Fig. S4a). The westerly phase of the QBO is strengthened in the Northern Hemisphere although the shift in latitude is smaller than for a 60 Tg eruption (cf. Fig. S10c and Fig. 10c) due to the smaller magnitude of eruption. For an eruption initiated during an e-QBO, the sulfate distribution is highly symmetrical and the largest change to the QBO is the increase in altitude of the phases.

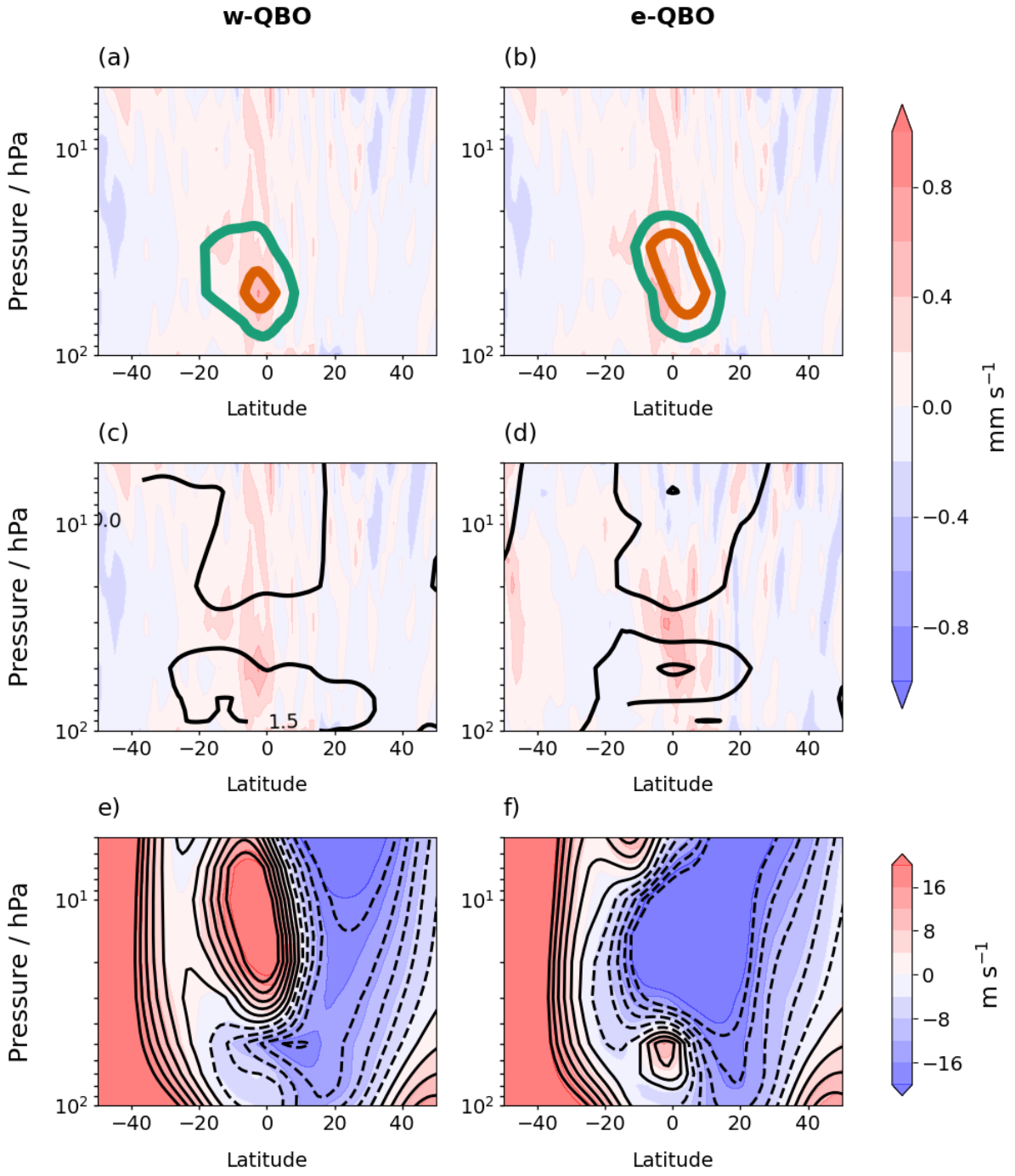

Figure S9: Two months after 15 Tg eruptions in July: (a), (b) shows the *w* anomalies (filled contours) and sulfate mass mixing ratio anomalies (coloured line contours) with respect to the control ensemble mean and (c), (d) shows the *w* anomalies (filled contours) and positive temperature anomalies (black solid contours). The sulfate mass mixing ratio contours are at interval of 5 x10^{-8}, 15 x10^{-8}, 50 x10^{-8} kg kg^{-1} and the temperature contours are in intervals of 1.5 K. Panels (e), (f) show the monthly mean zonal wind after the eruption (filled contours) compared to the control (black contours). The filled contour intervals are the same as the line contours, with dashed lines representing negative zonal winds in the line contours. Panels (a), (c) and (e) show results for the w-QBO, and panels (b), (d) and (f), for the e-QBO.

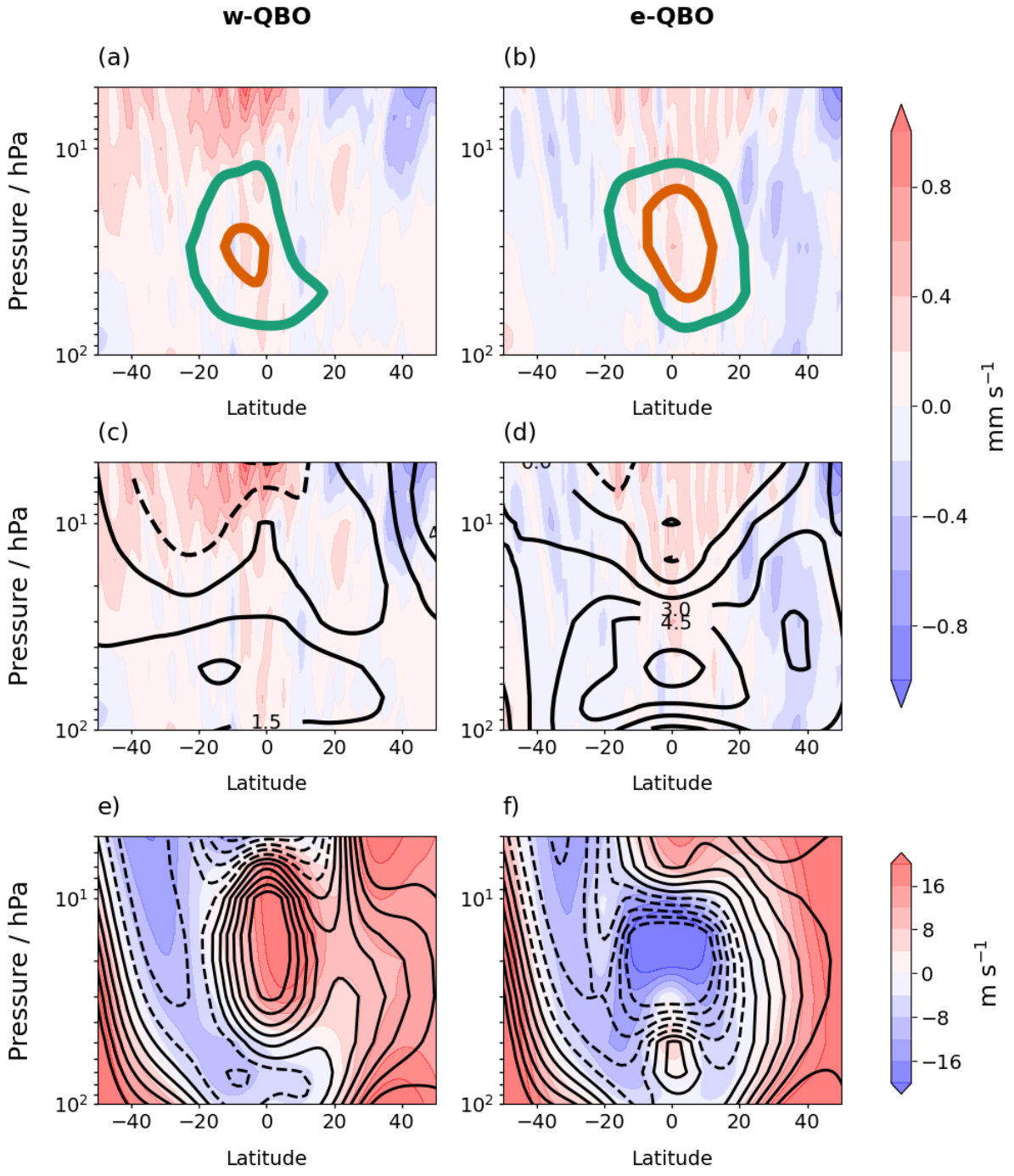

Figure S10: Five months after 15 Tg eruptions in July: (a), (b) shows the *w* anomalies (filled contours) and sulfate mass mixing ratio anomalies (coloured line contours) with respect to the control ensemble mean and (c), (d) shows the *w* anomalies (filled contours) and positive temperature anomalies (black solid contours). The sulfate mass mixing ratio contours are at interval of 5 x10^{-8}, 15 x10^{-8}, 50 x10^{-8} kg kg^{-1} and the temperature contours are in intervals of 1.5 K. Panels (e), (f) show the monthly mean zonal wind after the eruption (filled contours) compared to the control (black contours). The filled contour intervals are the same as the line contours, with dashed lines representing negative zonal winds in the line contours. Panels (a), (c) and (e) show results for the w-QBO, and panels (b), (d) and (f), for the e-QBO.

Supplementary Text 4: The latitudinal structure of the QBO

In addition to a shift in the latitude of the QBO westerly phase, the zonal winds may also change latitudinal structure following eruptions initiated during a w-QBO state. Fig. S11a and Fig. S11b show

that at 20 hPa, the zonal wind of the control simulation is approximately Gaussian whereas the zonal winds after an eruption show a secondary maximum at 18° S and 5° N, respectively.

As described in Sect. 3.3, an increase in westerly wind strength at subtropical latitudes relative to the control may be related to the temperature gradient created by the aerosol distribution. Fig. S11 shows the relationship between the sAOD, change in temperature curvature and change in zonal wind compared to the control at 20 hPa for eruptions initiated during a w-QBO in July and January. The movement of the westerly phase into the Northern Hemisphere for an eruption in July (Fig. S11a) and into the Southern Hemisphere for an eruption in January (Fig. S11b) can be identified, as well as a smaller 'secondary maximum' in the zonal wind in the opposite hemisphere. The increase in zonal wind in both hemispheres coincides with a decrease in sAOD; the changes being larger in the Northern Hemisphere for a July eruption and the Southern Hemisphere for a January eruption (Fig. S11c, S11d). It is likely that the decline in sulfate aerosol burden away from the equator has led to a temperature gradient that supports a westerly wind at higher latitudes. This is suggested by the increase in temperature curvature at 20 hPa, which coincides with the changes in sAOD (Fig. S11e, S11f). It is also likely that feedbacks are occurring so that changes to the zonal winds influence circulation of the aerosol, thereby sustaining the described relationship between aerosol, zonal wind and temperature.

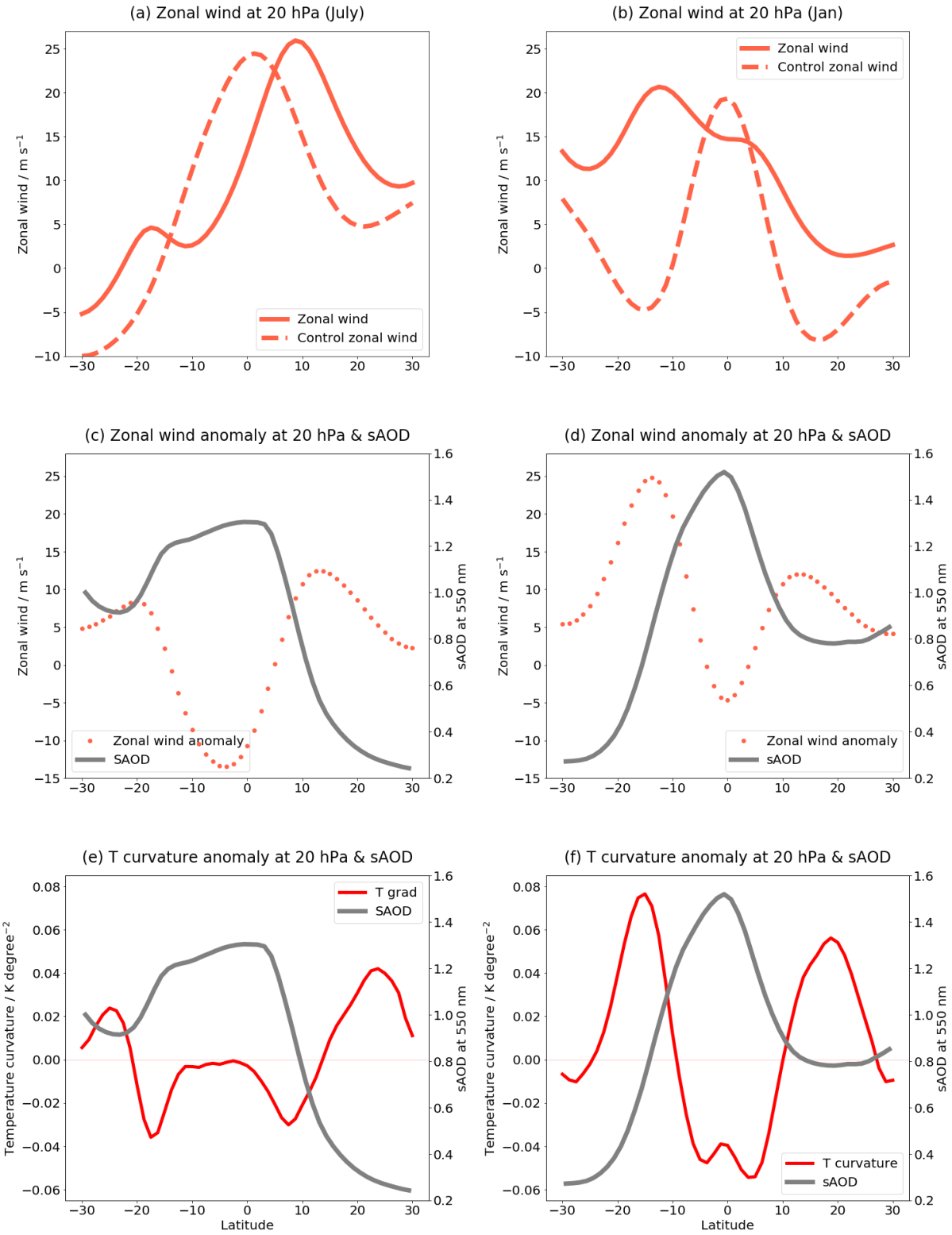

Figure S11: For a 60 Tg eruption initiated during a w-QBO, 5 months after the eruption (a, b) show the zonal wind for the control simulation (orange dashed line) and after an eruption (orange solid line), (c, d) show a comparison between zonal wind anomaly compared to the control simulation at 20 hPa (orange points) and sAOD (grey solid line), (e, f) show a comparison between SAOD (grey solid line) and latitudinal temperature gradient (red solid line). Column 1 shows results for an eruption initiated in July. Column 2 shows results for an eruption initiated in January.